ARTICLE

Check for updates

Journal of
Sensor Science and Technology

The Korean Sensors Society

A Kinematic Consistency-Based Method for Refining Axial Twist Errors in Skeleton-Based Motion Data

Inwon Choi[1], Mingyu Jang[2], and Jinhyun Kim[3,+]

[1]*School of Mechanical Engineering, Seoul National University of Science and Technology, 232 Gongneung-ro, Nowon-gu, Seoul, 01811, Republic of Korea*
[2]*Future Mechanical Technology Research Center, Seoul National University of Science and Technology, 232 Gongneung-ro, Nowon-gu, Seoul, 01811, Republic of Korea*
[3]*School of Mechanical and Automotive Engineering, Seoul National University of Science and Technology, 232 Gongneung-ro, Nowon-gu, Seoul, 01811, Republic of Korea*

Cite This: *J. Sens. Sci. Technol. Vol. 35, No. 1 (2026) 13-21*

https://doi.org/10.46670/JSST.2026.35.1.13

ABSTRACT: Optical motion capture is vital for the digitization of human movement, yet marker occlusion often causes unnatural axial twist errors in limb segments. Current refinement methods primarily target marker trajectories or general smoothing, leaving skeleton-based axial rotations inadequately addressed when raw marker data are absent. This study proposes a kinematic framework to automatically detect and refine these twist errors by analyzing the kinematic relationship between parent and child joints. We utilize swing–twist decomposition to isolate the parent joint's axial rotation and estimate the azimuth rotation to identify kinematic contradictions, such as counter-rotating joint behavior. Validation using synthetic level-shift errors injected into the CMU Motion Capture Database demonstrated a Frame Success Rate (FSR) of 94.81%. The proposed method significantly reduced the Mean Absolute Error (MAE) from 124.61° to 8.91°, effectively removing 92.85% of injected errors while preserving the global orientation of the motion. This approach ensures the kinematic integrity of skeleton animation, providing a robust solution for high-precision motion analysis tasks such as motion retargeting.

KEYWORDS: *Motion capture, Data refinement, Skeleton model, Kinematic consistency, Axial rotation, Swing–twist decomposition*

1. INTRODUCTION

Optical motion capture is a technology that converts human motion into the spatiotemporal poses of a digital body model, and it is widely used not only in the film and animation industries but also in diverse application fields such as games [1], medical rehabilitation [2], and sports analysis [3]. These applications require a human skeleton model, which is constructed in optical motion capture by attaching reflective markers to the body and estimating their positions using infrared cameras. In fields that demand high precision, high-quality motion data that preserve the continuity of joint rotations and kinematic consistency are essential, and the hierarchical structure of the skeleton and joint rotation information serve as fundamental components for representing captured motion.

In marker-based optical motion capture, constructing a human skeleton model requires at least three markers per limb segment [4,5], which is the minimum number needed to determine the positions of the joints at both ends of the segment as well as its rotational information. However, in practical motion capture environments, markers are frequently occluded by surrounding objects or body parts, leading to data loss. When markers attached near both ends of a segment are occluded, joint information in that region may be missing, resulting in corrupted position and rotation data. Moreover, when auxiliary markers attached to the bone are occluded, errors can arise specifically in axial rotation information. Fig. 1 illustrates a representative example of an axial twist error, in which an unintended twist at the LeftForeArm joint transforms an otherwise normal posture (a) into the distorted arm orientation shown in (b). In addition to marker occlusion

[+]Corresponding author: jinhyun@seoultech.ac.kr
Received : Dec. 30, 2025, Revised : Jan. 8, 2026, Accepted : Jan. 12, 2026

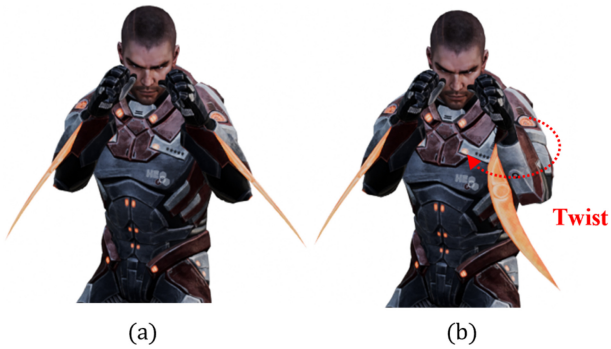

Fig. 1. Comparison of normal posture and axial twist error using a character model provided by Adobe Mixamo. (a) Normal posture, (b) Motion with an axial twist error.

[6], motion data can be degraded by various factors such as system noise [7], mislabeling [8], and soft tissue artefacts (STA) caused by skin and muscle motion [9]. Many previous studies have focused on refining marker-based motion data by reconstructing occluded marker positions [6], filtering sensor noise [7], relabeling markers [8], or on generating natural motion during skeleton construction through physics-based inverse kinematics (IK) optimization [9].

However, when motion capture data are not directly acquired from a capture system, it is often the case that only skeleton-based motion data are available without access to the original marker information. In such situations, existing methods designed for refining marker-based motion data cannot be effectively applied. In particular, there has been no prior work that explicitly models the loss of rotational information about the bone's longitudinal axis in skeleton models caused by occlusion of auxiliary markers. Furthermore, conventional physics-based IK optimization methods have inherent limitations in resolving axial rotational inconsistencies that occur along joint chains, often requiring manual intervention to remove visually unnatural motions.

To overcome these limitations, this study proposes a kinematic method that explicitly models constraints on axial rotation about the bone axis to automatically detect and refine twist errors in joint rotations. The proposed approach employs swing–twist decomposition to independently extract the twist component of the parent joint rotation about the parent–child axis. Simultaneously, the azimuthal change of the child joint about the same axis is estimated to analyze the directional consistency between the two rotations. By identifying kinematic contradictions based on mismatched rotational directions between the parent and child joints, the proposed algorithm detects erroneous segments. During refinement, the method is designed to preserve the continuity of the overall joint orientation, selectively correcting only the axial twist error component without introducing unnecessary pose distortions.

To the best of our knowledge, this study is the first to define and mathematically model axial twist errors by exploiting the kinematic consistency of joint chains in a skeleton-based motion data environment. Furthermore, by combining swing–twist decomposition with azimuthal rotation analysis, we propose a novel framework that effectively identifies and refines axial twist errors that are difficult to detect using conventional rotation analysis alone. The proposed method was validated on a large-scale benchmark dataset with synthetically injected errors, demonstrating its effectiveness in refining axial twist errors across a wide range of motions and joints. Quantitative results show that the proposed approach successfully removes axial twist errors and restores the original motion, and qualitative evaluation confirms that the refined motions align well with human visual intuition.

2. RELATED WORK

Optical motion capture data are susceptible to quality degradation due to various factors, including marker occlusion, incorrect marker labeling, and sensor noise. To address these issues, numerous studies over the past decades have focused on refining motion data either by reconstructing missing marker positions or by smoothing joint rotations in skeleton-based representations to improve overall motion quality. This section reviews existing approaches by categorizing them into interpolation and signal-processing methods, statistical modeling techniques, kinematic and physical constraint-based approaches, and recent learning-based methods. Their relevance to axial twist errors, which are the focus of this study, as well as their inherent limitations, are discussed.

2.1 Interpolation- and Signal Processing-Based Refinement Methods

Early motion data refinement studies mainly relied on mathematical interpolation of missing marker trajectories or frequency-domain filtering to suppress noise. Linear interpolation and spline-based methods are effective for filling short-term gaps and are computationally efficient, making them suitable for real-time applications. In particular, Howarth and Callaghan [10] compared various interpolation techniques and demonstrated that polynomial interpolation methods such as cubic splines and PCHIP are effective for restoring smooth human motion trajectories. Winter [11] also summarized standard approaches for removing high-frequency noise using low-pass filters such as the Butterworth filter.

However, these signal processing-based methods treat each

marker or joint angle as an independent time-series signal and do not explicitly consider the rigid-body kinematics of the human skeleton. As a result, they cannot detect physically implausible phenomena such as changes in inter-marker distances or biomechanically impossible joint configurations. More importantly, in cases such as the axial twist errors addressed in this study—where the data remain temporally continuous but exhibit biased values or drift—these methods tend to retain or amplify the error rather than separating it from valid motion components.

2.2 Statistical Modeling- and Matrix Completion-Based Methods

As motion capture datasets have grown in size, statistical techniques exploiting spatial and temporal correlations among markers have been proposed. Liu and McMillan [12] utilized principal component analysis (PCA) based on the observation that human motion resides in a low-dimensional subspace, allowing missing or corrupted markers to be reconstructed at statistically most probable locations. Low-rank matrix completion (LRMC) methods have also been extensively studied. Feng et al. [13] and Imamura et al. [14] represented motion data as matrices and effectively removed large-scale missing data and noise by minimizing the nuclear norm to reduce matrix rank.

While these statistical methods are powerful for recovering global motion patterns, they are computationally expensive and tend to over-smooth local kinematic details such as subtle joint rotations. Moreover, although they are highly effective at reconstructing three-dimensional marker positions, they provide limited guarantees that the joint orientations computed from reconstructed markers preserve kinematically valid axial rotations. Consequently, these approaches are difficult to apply directly to skeleton-based motion data without access to the original marker information.

2.3 Kinematic- and Physical Constraint-Based Refinement Methods

Beyond purely data-driven processing, several studies have incorporated physical and kinematic properties of the human body directly into the refinement process. Aristidou and Lasenby [6] proposed an algorithm that enforces joint limit constraints in real time during inverse kinematics to prevent anatomically implausible poses. Herda et al. [15] constrained the rotational range of complex joints such as the shoulder using quaternion field boundaries, while Svantesson and Bornold [16] applied joint rotation constraints during real-time inverse kinematics to prevent unrealistic joint motions. Dorfmüller [17] employed a Kalman filter to estimate the dynamic state of the human body model and reduce noise.

These model-based approaches offer the advantage of explicitly controlling bone lengths and joint angles. However, due to the numerical characteristics of inverse kinematics solvers, error compensation frequently occurs: to minimize marker position errors, the solver may unnaturally twist certain joint degrees of freedom to achieve a mathematical solution. Although such methods incorporate physical constraints, their relatively simple constraint formulations are not sufficient to recover lost axial rotation information, particularly twist components about the bone axis.

2.4 Learning-Based Motion Refinement Methods

More recently, deep learning models trained on large-scale motion datasets have become prominent in motion refinement research. Holden [18] introduced the concept of a neural solver that directly outputs clean joint angles from noisy marker inputs, demonstrating the potential to replace traditional inverse kinematics pipelines. Kucherenko et al. [19] employed recurrent neural networks such as LSTMs to learn temporal continuity in motion sequences and reconstruct missing marker trajectories. Kim et al. [20] further improved reconstruction accuracy for complex motion sequences by incorporating attention mechanisms to effectively leverage long-term temporal dependencies.

While learning-based approaches can generate highly natural motions by modeling the underlying data distribution, they suffer from overfitting issues in which motions absent from the training data—or intentionally rapid twisting motions—are incorrectly treated as noise and modified. Furthermore, due to their black-box nature, it is difficult to provide clear kinematic or physical explanations for why specific errors are corrected.

2.5 Proposed Method and Key Contributions

Previous studies have largely focused on reducing marker position errors or improving the visual smoothness of motion. However, when marker occlusion or soft tissue artefacts introduce positional errors, axial twist errors in skeleton-based motion data have not been explicitly identified or addressed, in cases where parent and child joints of a limb segment appear to rotate in opposite directions about the bone axis.

The proposed method precisely separates rotation components about the bone axis using quaternion-based swing–twist decomposition and analyzes the directional relationship between parent and child joints by tracking azimuthal changes of the child–grandchild vector. This enables

detection of motion segments in which inverse twist behavior occurs between parent and child joints, which are defined as twist error intervals. We further propose an analytic refinement algorithm that selectively removes only the erroneous axial twist component while preserving intended twist motion and maintaining the global pose of all joints.

3. PROPOSED METHOD

This section proposes a method for defining, detecting, and correcting axial twist errors in skeleton-based motion data. Section 3.1 defines axial twist errors at joints. Section 3.2 describes how axial twist components are extracted separately for parent and child joints, and Section 3.3 presents the procedure for detecting and refining twist errors by combining these components.

3.1 Definition of Twist Error

Skeleton-based motion data are represented as a kinematic model with a hierarchical parent–child joint structure. In particular, the global orientation of each joint is defined by the relative local rotation of a child joint J_C with respect to its parent joint J_P according to forward kinematics. Under normal motion, when a twist occurs at the parent joint about the bone axis aligned with the segment's longitudinal direction, the child joint should rotate about the same axis, resulting in a corresponding change in pose in the global coordinate frame.

However, during motion capture, auxiliary markers used to determine rotational information may become occluded. When this occurs, rotational information about the segment's longitudinal axis can be temporarily lost, leading to unintended twist values at the affected frame. In such cases, a sudden twist change is observed in the global orientation of the parent joint, which dictates the segment's orientation, while the global orientations of the child joint and its downstream joints remain nearly unchanged. From a kinematic perspective, this implies that the local coordinate frame of the child joint has rotated in the opposite direction to cancel the parent's twist. This results in adjacent joints twisting in opposite directions, a motion that is physically implausible given the human skeletal structure.

Fig. 2 illustrates a representative example of a twist error. If a normal axial rotation occurs at J_P about the parent–child axis, the child joint and the downstream grandchild joint J_{GC} should rotate together, placing the grandchild at its ideal position J_{GC}^{ideal}. In contrast, when a twist error occurs, a counter-rotation at J_C cancels the rotation of J_P, causing the actual grandchild position J_{GC}^{real} to remain unchanged.

In this study, such behavior is defined as an axial twist error

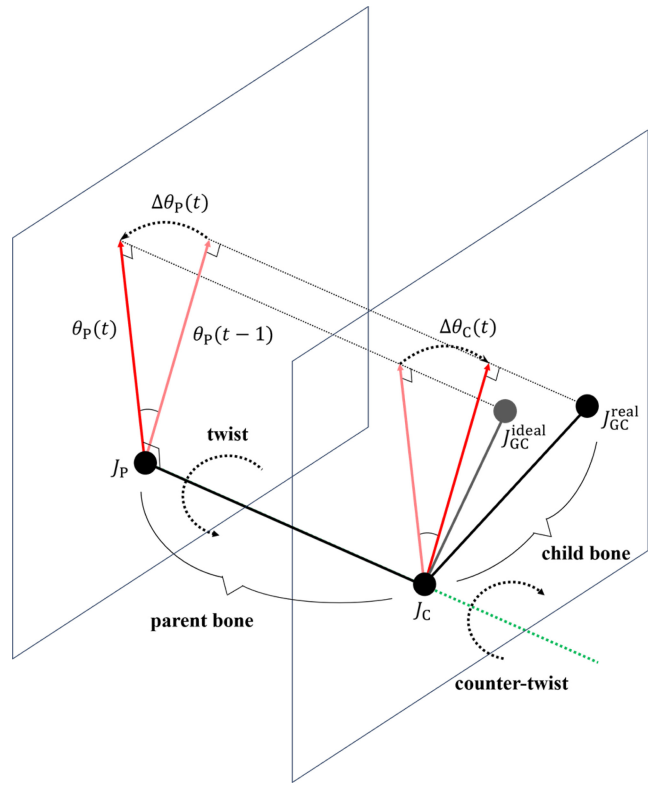

Fig. 2. Illustration of inverse axial twists between parent and child joints causing kinematic inconsistency.

and is mathematically expressed as:

$$\Delta\theta_P(t)\Delta\theta_C(t) < 0 \tag{1}$$

where $\Delta\theta_P(t)$ and $\Delta\theta_C(t)$ denote the frame-to-frame twist variations of the parent joint J_P and the child joint J_C, respectively, measured about the parent–child axis.

3.2 Extraction of Axial Twist Components at Each Joint

To quantitatively identify twist errors, twist components must be extracted independently from the parent and child joints. This section describes the extraction methods applied to each joint.

3.2.1 Twist Component Extraction at the Parent Joint

The twist component at the parent joint is defined with respect to the bone axis connecting the parent and child joints. To separate this component, quaternion-based swing–twist decomposition is employed.

Swing–twist decomposition [21] separates a rotation into a swing component, which is orthogonal to the axis, and a twist component, which rotates about the axis. The local rotation of the parent joint is represented by a quaternion q_P, and the unit

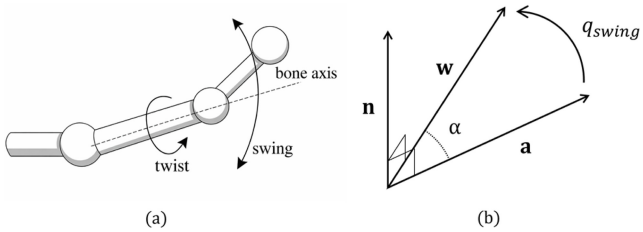

Fig. 3. Swing–twist decomposition about the bone axis. (a) swing and twist components, (b) geometric construction for computing q_{swing}.

vector **a** pointing from the parent to the child joint is defined as the twist axis. The quaternion q_{P} is decomposed into a swing component q_{swing} and a twist component q_{twist}, as expressed in:

$$q_{\text{P}} = q_{\text{swing}} q_{\text{twist}} \tag{2}$$

The twist component is computed using the direct method. As illustrated in Fig. 3, when the parent rotation quaternion q_{P} rotates the initial vector **a** to

$$\mathbf{w} = q\mathbf{a}q^{-1} \tag{3}$$

the swing quaternion q_{swing} is defined as the minimum-angle rotation that maps **a** to **w**. The rotation axis of the swing is given by

$$\mathbf{n} = \frac{\mathbf{a} \times \mathbf{w}}{\|\mathbf{a} \times \mathbf{w}\|} \tag{4}$$

and the angle between the two vectors is

$$\cos\ \alpha = \mathbf{a} \cdot \mathbf{w} \tag{5}$$

Using these quantities, the swing component is computed as

$$q_{\text{swing}} = \cos\left(\frac{\alpha}{2}\right) + \sin\left(\frac{\alpha}{2}\right)\mathbf{n} \tag{6}$$

Accordingly, the twist component of the parent rotation is obtained by explicitly removing the swing component from the original rotation:

$$q_{\text{twist}} = q_{\text{P}} q_{\text{swing}}^{-1} \tag{7}$$

The twist angle about axis **a** is then computed from the twist quaternion via quaternion-to-angle conversion:

$$\theta_{\text{P}} = 2\text{atan2}(\|(q_{\text{twist}})_v\|, (q_{\text{twist}})_w) \tag{8}$$

As shown in Fig. 4, θ_{P} represents the pure axial rotation about **a**. Finally, the frame-to-frame twist variation at the parent joint is computed as

$$\Delta\theta_{\text{P}}(t) = \theta_{\text{P}}(t) - \theta_{\text{P}}(t-1) \tag{9}$$

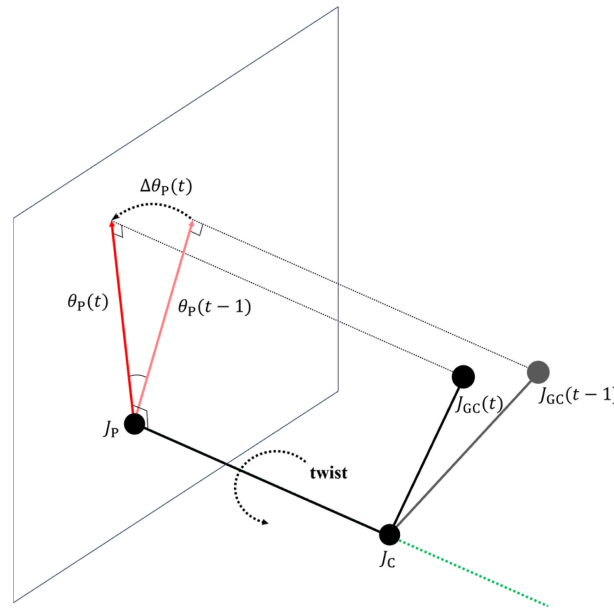

Fig. 4. Extraction of the axial twist component at the parent joint using swing–twist decomposition.

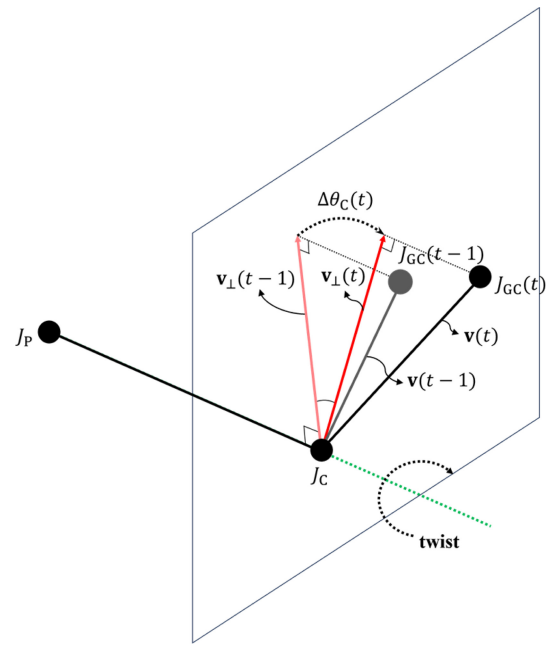

Fig. 5. Estimation of the child joint twist via azimuth variation of the child–grandchild vector.

3.2.2 Twist Component Estimation at the Child Joint

For the child joint, it is difficult to directly extract the twist about the parent–child axis using swing–twist decomposition on its local rotation. Therefore, this study estimates the child joint's twist using an alternative approach.

First, the child–grandchild vector is calculated in the parent joint's coordinate frame, as shown in Fig. 5:

$$\mathbf{v}(t) = \mathbf{R}_C(t)\mathbf{b}_{GC} \tag{10}$$

Where $\mathbf{R}_C(t)$ is the rotation matrix of the child joint, and $\mathbf{b}_{GC}$ is the offset vector from the child joint to the grandchild joint. The vector $\mathbf{v}(t)$ is then projected onto the plane orthogonal to the parent–child axis, and the temporal variation of the azimuth angle of the projected vector is used to estimate the twist component of the child joint.

$$\mathbf{v}_\perp(t) = \mathbf{v}(t) - (\mathbf{v}(t)\cdot\mathbf{a})\mathbf{a} \tag{11}$$

$$\theta_C(t) = \text{atan2}((\mathbf{v}_\perp(t-1)\times\mathbf{v}_\perp(t))\cdot\mathbf{a}, \mathbf{v}_\perp(t-1)\cdot\mathbf{v}_\perp(t)) \tag{12}$$

3.3 Error Detection and Refinement

Using the parent and child twist variations obtained above, twist errors are detected and corrected.

3.3.1 Twist Error Detection

Based on the kinematic characteristics defined earlier, twist error intervals are characterized by rapid changes in twist with opposite signs at the parent and child joints. Therefore, frames satisfying the inequality $\Delta\theta_P(t)\Delta\theta_C(t) < 0$ are considered candidates for twist error occurrence. To prevent overcorrection, only the smaller magnitude of the two twist variations is selected as the error magnitude, ensuring that intended twist motion is preserved while removing inverse twist behavior. A threshold τ is also introduced to exclude sensor noise and minor fluctuations.

$$m(t) = \min(|\Delta\theta_P(t)|, |\Delta\theta_C(t)|),\ m(t) \geq \tau \tag{13}$$

Twist errors do not typically appear as instantaneous, single-frame events. Instead, they manifest as level-shift-type errors, where a constant offset is introduced over a continuous interval between the onset and resolution of marker occlusion. Accordingly, an error magnitude function $\text{err}(t)$ and a cumulative offset function $\text{offset}(t)$ representing the parent's twist offset are defined. When an error event occurs, $\text{err}(t)$ is added to $\text{offset}(t)$. Otherwise the offset is maintained as $\text{offset}(t) = \text{offset}(t-1)$, ensuring consistent correction over the entire error interval.

3.3.2 Twist Error Removal with Preservation of Child Orientation

For detected error intervals, the twist component of the parent joint is corrected. If only the parent joint's twist is modified, the hierarchical structure causes unintended changes in the global orientation of the child joint. However, by definition, the global orientation of the child joint must be preserved when correcting axial twist errors.

Let $q(t)$ and $q'(t)$ denote the joint rotations before and after correction, respectively. The following constraint is enforced:

$$q_P(t)q_C(t) = q'_P(t)q'_C(t) \tag{14}$$

From this relationship, the corrected rotation of the child joint is obtained as

$$q'_C(t) = (q'_P(t))^{-1}q_P(t)q_C(t) \tag{15}$$

Through this procedure, the overall skeleton pose is preserved while selectively removing only the erroneous axial twist component.

4. EXPERIMENTS AND RESULTS

This section quantitatively evaluates the performance of the proposed skeleton-based twist error detection and refinement method. The experiments were conducted by injecting synthetic twist errors into normal motion data with known ground truth, restoring the corrupted data using the proposed algorithm, and quantitatively comparing the refined results with the original motions.

4.1 Experimental Data Configuration

To objectively evaluate the performance of the proposed method, the CMU Motion Capture Database [22] was used. As the CMU database is originally provided in ASF/AMC format, we utilized the dataset converted into the BVH format by Bruce Hahn [23]. The experimental dataset consists of a total of 2,548 BVH motion files, including a wide variety of motion types such as walking, running, jumping, dancing, and fighting, thereby reflecting diverse motion characteristics.

4.1.1 Definition of Target Joints for Synthetic Error Generation

Limb segments in which twist errors may occur when auxiliary markers are occluded—specifically, segments with three markers attached—were selected as target joints. For each BVH file, two joints were selected while excluding joints that form a continuous chain. The target joints include the Shoulder, Arm, and ForeArm in the upper body, and the UpLeg and Leg in the lower body.

4.1.2 Sampling of Error Intervals

When auxiliary markers are occluded, twist errors are generated as level-shift-type errors, where an offset is introduced over a continuous frame interval. Accordingly, for each target joint, between two and five twist error intervals were randomly generated, each spanning 1 to 20 frames with twist offsets ranging from ±5° to 180°.

4.1.3 Error Injection Method

Using swing–twist decomposition, the sampled offset was added only to the twist component of the local rotation of each target joint. To ensure that the global orientation of the child joint remained unchanged, the inverse of the parent joint rotation, $(q'_P(t))^{-1}$, was multiplied with the original child rotation. This process reproduces a kinematic effect that is equivalent to a real twist error.

In cases where the child joint is the Hand, multiple joints correspond to the grandchild. Therefore, the unit vector along the Z-axis of the Hand coordinate frame was used as the child–grandchild vector $\mathbf{b}_{GC}$.

4.2 Experimental Results

4.2.1 Quantitative Performance Evaluation

To evaluate the refinement performance of the algorithm, the Mean Absolute Error (MAE) and Root Mean Square Error (RMSE) of joint rotation angles were measured before and after refinement. In addition, the Frame Success Rate (FSR) was introduced to assess the reliability of the algorithm. FSR is defined as the proportion of frames with twist errors in which the absolute rotation error was reduced by at least 80%.

When the proposed algorithm was applied to the entire synthetic dataset, the overall average refinement performance is summarized in Table 1. Out of a total of 335,004 error frames, 317,611 frames were successfully refined, corresponding to an FSR of approximately 94.81%, indicating that twist errors were effectively removed in most frames. Furthermore, the average MAE was significantly reduced from 124.61° before refinement to 8.91° after applying the proposed method, while the RMSE decreased from 160.28° to 39.96°. These results indicate that 92.85% of the initially injected errors were effectively removed, demonstrating that the proposed method robustly corrects twist errors using only the kinematic information of the skeleton, without requiring marker data.

4.2.2 Joint-wise Performance Analysis

To analyze variations in refinement performance according to joint kinematic characteristics, the Residual Error Ratio (RER) and Frame Success Rate (FSR) were computed individually for each joint.

Table 1. Overall quantitative performance of twist error refinement

Metric	Before Refinement	After Refinement	Performance Improvement
MAE (deg)	124.61	8.91	92.85% reduction
RMSE (deg)	160.28	39.96	75.06% reduction
FSR (%)	–	–	94.81%

Table 2. Detailed performance metrics across limb segments

Side	Segment	MAE After (°)	RER (%)	FSR (%)
Left	Shoulder	1.39	1.34	99.12
	Arm	12.79	8.78	92.80
	ForeArm	1.46	1.38	98.97
	UpLeg	39.39	26.38	79.66
	Leg	2.53	2.20	98.15
Right	Shoulder	1.65	1.73	98.88
	Arm	5.74	3.44	96.46
	ForeArm	1.81	1.81	98.11
	UpLeg	31.40	21.77	82.38
	Leg	2.22	2.32	98.03

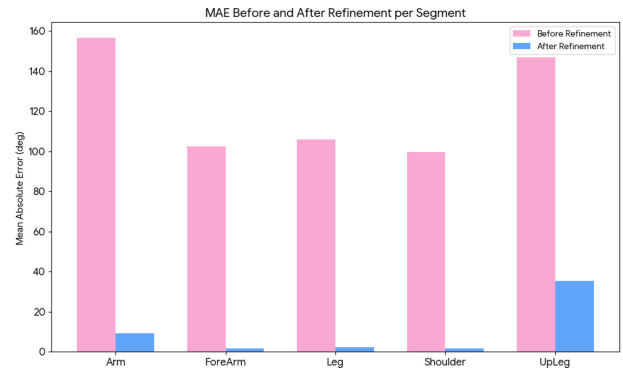

Fig. 6. Comparison of Mean Absolute Error (MAE) before and after the proposed refinement for each limb segment.

As shown in Table 2 and Fig. 6, the ForeArm, Leg, and Shoulder joints achieved very high FSR values exceeding 98%, with RER values of approximately 1–2%, indicating near-perfect restoration performance. The Arm joint, which has a relatively wide range of motion, also demonstrated stable performance with success rates of approximately 92–96%. In contrast, the UpLeg joint exhibited a relatively lower FSR of around 80% and an RER exceeding 20%. This behavior can be attributed to the fact that during motions such as leg extension, the child–grandchild vector becomes nearly aligned with the parent–child axis, causing azimuth estimation to become unstable more frequently than in other joints. Nevertheless, the achievement of success rates exceeding 90% for most major joints, excluding these singular cases, strongly supports the effectiveness of the proposed method.

4.2.3 Discussion

The proposed method effectively detected and refined both abrupt spike-type distortions and discontinuous level-shift intervals caused by twist errors. In particular, by selectively

removing only local axial rotation errors while preserving the overall motion trajectory, the method successfully restored the original motion without introducing the information loss or phase lag typically introduced by low-pass filtering approaches, especially in fast movements.

However, to further improve robustness near kinematic singularities—such as configurations in which the parent–child–grandchild joints become collinear—future work will be required. Potential directions include incorporating additional auxiliary indicators beyond azimuth estimation or enhancing exception-handling strategies near singular configurations.

5. CONCLUSION

This study analyzed kinematic inconsistencies that arise in skeleton-based motion data and proposed a novel framework for defining, automatically detecting, and correcting twist errors. The proposed method combines swing–twist decomposition with azimuth estimation to characterize the relationship between axial rotations of the parent joint about the bone axis and corresponding inverse rotations of the child joint, enabling the detection of abnormal twist behavior at individual joints.

The significance of this work lies in explicitly modeling anomalous phenomena in motion capture data as single-joint axial twist errors defined with respect to the bone axis and establishing a kinematic framework to resolve them. In particular, the proposed approach overcomes the limitations of conventional signal processing-based methods, such as low-pass filtering, which rely on frequency characteristics and therefore tend to either suppress meaningful high-frequency motion components or fail to detect low-frequency drift errors. By directly identifying structural kinematic contradictions between joints, the proposed method selectively removes only erroneous twist components regardless of their temporal duration or frequency characteristics, while preserving the dynamic properties and overall global pose of the original motion through kinematic correction.

Experimental results demonstrate that the proposed method achieves an overall FSR of 94.81%, with success rates exceeding 96% for major joints such as the arms and legs. Nevertheless, limitations were observed in cases where the parent–child axis and the child–grandchild axis approach collinearity, as in thigh segments, which leads to reduced accuracy in azimuth estimation. Future work will focus on improving robustness in such kinematic singular configurations by introducing multi-chain kinematic constraints that incorporate information from adjacent joints or by integrating learning-based estimation models to further enhance the algorithm's robustness.

In conclusion, the kinematic refinement algorithm proposed in this study serves as an effective post-processing method for improving the reliability of skeleton-based motion data and contributes to enhanced data quality in computer graphics and animation applications. Furthermore, the kinematic consistency-based detection logic established in this work can be extended to serve as physical constraints or loss functions in deep learning-based motion generation and reconstruction models, with the potential to improve kinematic integrity across a wide range of application domains.

CRediT Authorship Contribution Statement

Inwon Choi: Conceptualization, Methodology, Investigation, Data curation, Software, Writing – original draft. **Mingyu Jang:** Conceptualization, Investigation, Data curation, Software, Methodology, Validation. **Jinhyun Kim:** Supervision, Formal analysis, Writing – review and editing, Funding acquisition.

Declaration of Competing Interest

The authors declare that they have no known competing financial interests or personal relationships that could have appeared to influence the work reported in this paper.

Acknowledgements

This research was supported by the "Regional Innovation System & Education (RISE)" through the Seoul RISE Center, funded by the Ministry of Education (MOE) and the Seoul Metropolitan Government (2025-RISE-01-014-04).

This paper was supported by Korea Institute for Advancement of Technology(KIAT) grant funded by the Korea Government(MOTIE) (RS-2024-00406796, HRD Program for Industrial Innovation).

REFERENCES

[1] E.S.L. Ho, T. Komura, C.L. Tai, Spatial relationship preserving character motion adaptation, ACM Trans. Graph. 29 (2010) 33.

[2] A. Leardini, F. Biagi, A. Merlo, C. Belvedere, M.G. Benedetti, Multi-segment trunk kinematics during locomotion and elementary exercises, Clin. Biomech. 26 (2011) 562–571.

[3] X. Suo, W. Tang, Z. Li, Motion Capture Technology in Sports Scenarios: A Survey, Sensors 24 (2024) 2947.

[4] OptiTrack, Skeleton Tracking. https://docs.optitrack.com/motive/skeleton-tracking, 2025 (accessed 26 December 2025).

[5] Vicon, Plug-in Gait Reference Guide. https://help.vicon.com/space/Nexus218/406491281/Plug-in+Gait+Reference+Guide, 2025 (accessed 26 December 2025).

[6] A. Aristidou, J. Lasenby, Real-time marker prediction and

CoR estimation in optical motion capture, Vis. Comput. 29 (2013) 7–26.
[7] E. Martini, A. Calanca, N. Bombieri, Denoising and completion filters for human motion software: a survey with code, Comput. Sci. Rev. 58 (2025) 100780.
[8] J. Meyer, M. Kuderer, J. Müller, W. Burgard, Online marker labeling for fully automatic skeleton tracking in optical motion capture, Proceedings of the IEEE International Conference on Robotics and Automation, Hong Kong, China, 2014, pp. 5652–5657.
[9] S. Duprey, A. Naaim, F. Moissenet, M. Begon, L. Chèze, Kinematic models of the upper limb joints for multibody kinematics optimisation: An overview, J. Biomech. 62 (2017) 87–94.
[10] S.J. Howarth, J.P. Callaghan, Quantitative assessment of the accuracy for three interpolation techniques in kinematic analysis of human movement, Comput. Methods Biomech. Biomed. Engin. 13 (2010) 847–855.
[11] D.A. Winter, Biomechanics and Motor Control of Human Movement, fourth ed., Wiley, Hoboken, 2009.
[12] G. Liu, L. McMillan, Estimation of missing markers in human motion capture, Vis. Comput. 22 (2006) 721–728.
[13] Y. Feng, J. Xiao, Y. Zhuang, X. Yang, J.J. Zhang, R. Song, Exploiting temporal stability and low-rank structure for motion capture data refinement, Inf. Sci. 277 (2014) 777–793.
[14] R. Imamura, M. Okuda, MOCAP signal interpolation using low-rank matrix recovery, Proceedings of the Asia-Pacific Signal and Information Processing Association Annual Summit and Conference, Honolulu, USA, 2018, pp. 871–874.
[15] L. Herda, R. Urtasun, P. Fua, A. Hanson, Automatic Determination of Shoulder Joint Limits Using Quaternion Field Boundaries, Int. J. Rob. Res. 22 (2003) 419–436.
[16] J. Svantesson, J. Bornold, A Real-Time Adaptation of Inverse Kinematics for Motion Capture, Master's thesis, Chalmers University of Technology, Göteborg, Sweden, June 2015.
[17] K. Dorfmüller-Ulhaas, Robust Optical User Motion Tracking Using a Kalman Filter, Technical Report 2003-06, University of Augsburg, Augsburg, Germany, May 2003.
[18] D. Holden, Robust solving of optical motion capture data by denoising, ACM Trans. Graph. 37 (2018) 1–12.
[19] T. Kucherenko, J. Beskow, H. Kjellström, A Neural Network Approach to Missing Marker Reconstruction in Human Motion Capture, ArXiv., https://arxiv.org/abs/1803.02665 (2018).
[20] S.U. Kim, H. Jang, H. Im, J. Kim, Human motion reconstruction using deep transformer networks, Pattern Recognit. Lett. 150 (2021) 162–169.
[21] P. Dobrowolski, Swing-twist decomposition in Clifford algebra, ArXiv., https://arxiv.org/abs/1506.05481 (2015).
[22] Carnegie Mellon University, CMU Graphics Lab Motion Capture Database. http://mocap.cs.cmu.edu/, 2025 (accessed 26 December 2025).
[23] B. Hahne, The Motionbuilder-friendly BVH conversion release of the Carnegie-Mellon University (CMU) Graphics Lab Motion Capture Database. https://sites.google.com/a/cgspeed.com/cgspeed/motion-capture/the-motionbuilder-friendly-bvh-conversion-release-of-cmus-motion-capture-database, 2010 (accessed 26 December 2025).